Review Article

A Brief Study of Magnesium-Zinc Alloy Scaffolds Performance

Z. S. Seyedraoufi*

Advanced Materials Engineering Research Center, Karaj Branch, Islamic Azad University, Karaj, Iran.
Received: 01 March 2022 - Accepted: 10 June 2022

Abstract

Due to good biocompatibility, corrosion and mechanical properties, magnesium (Mg) is considered promising degradable material for orthopedic applications. In this work, Mg-Zn alloy scaffolds were produced via powder metallurgy method. The microstructure, composition, in vitro corrosion and mechanical properties of magnesium-zinc alloy scaffolds were investigated. The X-ray diffraction (XRD) results indicated the formed nano precipitates consist of MgZn and $MgZn_2$ intermetallics that dispersed in αMg. The scanning electron microscopy (SEM) images proved that Mg-Zn intermetallics nano precipitates with round morphology and size of 20–50 nm are homogenously dispersed in the αMg matrix. The results showed that the addition of Zn element increases the compressive strength, Young's modulus and hardness. Also, Mg-(x)Zn alloy scaffolds produced, improved the in vitro anti-corrosion property of the αMg. The best unti-corrosion property is obtained with 3% Zn and further increase of Zn content up 4% deteriorates the corrosion property. All the results suggest that the Mg-Zn alloy scaffolds have the potential to serve as degradable implants for bone substitute applications.

Keywords: Magnesium-Zinc Alloy, Scaffold, In Vitro Corrosion, Mechanical Properties.

1. Introduction

One of the most attractive subjects in tissue engineering is the development of a scaffold, a 3D solid structure that plays a key role in assisting tissue regeneration [1]. Ideally, a scaffold must be porous, bioactive, and biodegradable and possess adequate enough mechanical properties to the biological site. Sufficient porosity is needed to accommodate cell proliferation and differentiation, which will eventually enhance tissue formation [1, 2]. A bioactive scaffold promotes cell-biomaterial interactions, cell proliferation, adhesion growth, migration, and differentiation. A biodegradable scaffold allows the replacement of biological tissues via physiological extracellular components without leaving toxic degradation products. Its degradation rate should match the regeneration rate of new tissue in order to maintain the structural integrity and to provide a smooth transition of the load transfer from the scaffold to the tissue [2]. Finally, as a mechanical support, a scaffold must be provided adequate mechanical stability to withstand both the implantation procedure and the mechanical forces that are typically experienced at the scaffold-tissue interface and does not collapse during patient's normal activities [2]. Mechanically, the major challenge is to achieve adequate initial strength and stiffness and preserving them during the stages of healing or neotissues production throughout the scaffold degradation process [2-5].

*Corresponding author
Email address: z.seyedraoufi@kiau.ac.ir

Porous designing of Mg-based scaffold has been proven to play a significant role in cell growth and proliferation. Also, Mg is largely found in bone tissue, it is an essential element to human body, and its presence is beneficial to bone growth and strength [5-8]. Owing to their good biocompatibility and rather low mechanical stiffness (i.e., low Young's modulus), Mg-alloys are potential candidates for biodegradable implants [9, 10]. However, the problem with most of Mg-alloys is their exceedingly high corrosion rates in physiological conditions, which makes their biodegradability to be faster than the time required to heal the bone [11]. For this reason it is important to decrease the degradation rate of magnesium alloys using different techniques such as purification, alloying, surface coating [12, 13].

Mg is usually alloyed with other elements or used as composites. Enhanced mechanical properties have been reported in Mg composite reinforced with nanoscaled particles such as SiC, Al_2O_3 and AlN. The demand for greater performance of the Mg alloys or composites leads to the development of Mg-based metal matrix composite (MMC) with nanocrystalline microstructure reinforced by in-situ particles. Other alloying elements has been studied for developing biodegradable Mg-alloys with good mechanical and corrosion properties [14]. Zn is selected as the alloying element to achieve the good biocompatibility and Zn is necessary microelement and component of many proteins, nucleic acid synthetase of human body. Also Zn can accelerate the metabolism of cells. The addition of Zn to Mg for producing the Mg-Zn alloy improves both the

mechanical properties and the corrosion resistance of magnesium alloys [14-18]. It has been shown that Mg–Zn alloys possess the highest capacity for precipitation hardening due to segregation of an intermediate phase that ensures a combination of high strength and ductility [17].
In this work, Mg powder is allowed to react with Zn powder at a temperature below the melting point of Mg. During fabrication, an Mg matrix is produced, and also Zn reacts with Mg to form the Mg–Zn intermetallic phases. Mg–Zn intermetallics in situ products serve as reinforcements and strengthening to toughen the αMg. In this work, porous Mg–Zn specimens containing different zinc amounts (1, 2, 3 and 4 wt %) have been fabricated using a powder metallurgy process. The microstructures, the mechanical and in vitro corrosion properties of the specimens are investigated.

2. Materials and Methods

Pure Zn (purity ≥99.8%, particle size ≤45μm) and pure Mg (purity ≥99%, particle size ≤100μm) powders purchased from Merck were utilised as starting materials. Urea particles purchased from Merck with a purity of 99.9% were used as the space-holder. The particle size of the spacer agent material was in the range of 200-400μm. After mixing the starting materials with the space-holder particles, porous Mg-Zn_x (x= 1, 2, 3 and 4 wt. %) samples were prepared via a powder metallurgy method. The mixtures of Mg and Zn powder were prepared based on 1, 2, 3 and 4 wt. % Zn, while the urea particles were thoroughly added to the above specimens with volume content of 15%. The mixed powder was uniaxially pressed at a pressure of 200MPa into green compacts 10 mm in diameter and 10 mm in length. The green compacts were then heat treated to burn out the spacer particles, and to sinter into the Mg Scaffolds in a tube furnace under an argon atmosphere. The heat-treatment process consists of two steps, i.e. at 250°C for 4h and 550°C for 2h.
Chemical composition of the specimens was performed by X-ray diffractometer (XRD: Philips 1800PW) with Cu Kα radiation. Morphology and element composition of the samples were identified by scanning electron microscopy (SEM: Tscan–Vega) equipped with energy dispersion spectroscopy (EDS) facility.
The compressive strength and the Young's modulus of the scaffolds was measured using compression testing of samples with dimensions of Φ10 mm × 15 mm. The tests were performed with a SANTAM (STM-20, Iran) testing machine at room temperature at a rate of 0.3mm/s. Each result was taken as the mean value of testing on five samples. The samples were examined by a micro-hardness testing machine made by the Iran-Copa company and MH3 model under a load of 100 grams for 15-second stoppage time. Pore sizes and geometric shapes of the synthesized alloy scaffolds were observed using optical microscopy. Total porosity (Π) of the scaffolds was measured using gravimetry according to the Eq. (1). [19]:

$$\Pi = (1 - \rho/\rho_s) \times 100\% \qquad \text{Eq. (1).}$$

Where ρ_s is the density of the Mg-Zn specimen evaluated via the immersion method and ρ is the apparent density of the porous Mg-Zn specimen, which can be measured by the weight divided by the volume of the porous specimen. The potentiodynamic polarization curves were obtained using a potentiostat (Autolab/PGSTAT302N) at a constant voltage scan rate of 5mv.s–l. Experiments were carried out in SBF at 37°C. A three-electrode cell with the samples as the working electrodes was used for the electrochemical measurements. The reference electrode was an Ag–AgCl electrode and the counter electrode was made of platinum. The area of the working electrode exposed to the solution was 0.85cm2. The composition and preparation procedure of SBF were as reported in Ref. [20]. The solution was buffered at pH of 7.4 using tris-hydroxymethyl aminomethane ($(HOCH_2)_3CNH_2$) and HCl at 37°C. Each result was taken as the mean value of testing on five samples.

3. Result and Discussion

3.1. Microstructure and Composition of Scaffolds

According to Eq. (1), the measured porosities of the synthesized scaffolds are presented in Fig. 1.

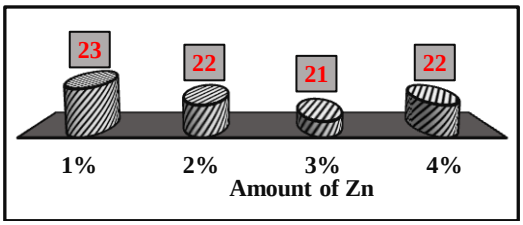

Fig. 1. Porosity of the synthesized scaffolds containing of different Zn amounts.

The optical micrograph of the synthesized Mg-2wt.% Zn scaffold is shown in Fig. 2. The average porosity of the specimen is 22%. It can be seen from Fig. 1. that there are two kinds of pores in the synthesized scaffolds, i. e. open interpenetrated macro pores and small isolated micro pores distributed within the matrix and resulted from the volume shrinkage during the sintering process of the Mg powders. The macro pores are in the size range of 200-400 μm. Fig. 3. shows the X-ray diffraction patterns of the cross-section of the sintered Mg-Zn scaffolds with the different contents of Zn. As seen in the patterns, Mg peaks were detected in all of the specimens, and MgO was detected in all of the patterns. In fact, the detected MgO peaks indicate that MgO was most likely formed during the preparation and/or sintering process.

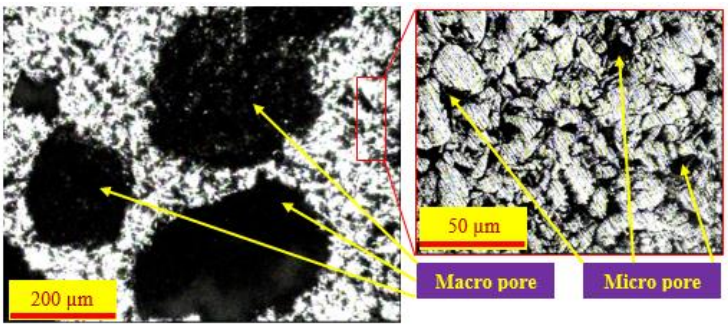

Fig. 2. The optical micrograph of the synthesized Mg-2wt.% Zn scaffold.

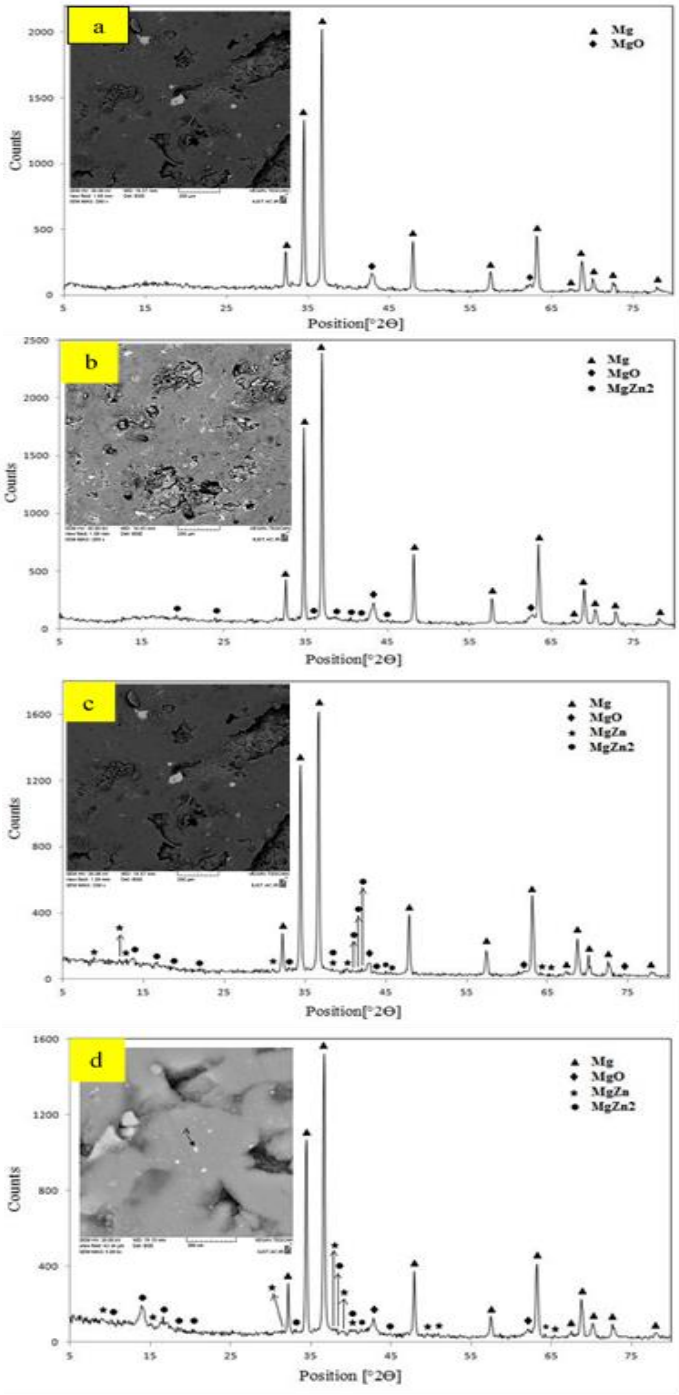

Fig. 3. The XRD patterns and SEM images of the synthesized scaffolds containing different Zn amounts: (a) 1, (b) 2, (c) 3 and (d) 4 wt. %.

Also, XRD results show that the formation of $MgZn_2$ and MgZn intermetallics are begun from 2 and 3 wt. %, respectively. As observed in the patterns, the peak intensity of intermetallics increases with addition of Zn content. When a cold-pressed Mg–Zn specimen is sintered in an argon atmosphere at temperature between 400 and 550℃, the possible chemical reactions during heating and solidification are given by Eq. (2), Eq. (3) and Eq. (4):

Zn (s) → Zn (l) Eq. (2).

Mg (s) + Zn (l) → Mg-Zn (l) Eq. (3).

Mg-Zn (l) → Mg (s) + MgxZny (s) Eq. (4).

It is expected that Reaction (2) will occur at about 410℃. As the sintering temperature increases to about 530℃, liquid-Zn in the product reacts with Mg to form the molten Mg–Zn alloy [15].

The SEM image of microstructure of the synthesized Mg-4wt.% Zn scaffold. As observed in the SEM micrograph, there are three phases. The black, bright and white regions belong to porosity, Mg matrix and Mg-Zn intermetallics. As can be seen the average particle size of the white particles is 20 nm.

EDS analysis of point A in Fig. 3.d is presented in Fig. 4. As observed this white nano particles contains of Mg and Zn elements and according to the results, formation of nano Mg-Zn intermetallics in the scaffolds is confirmed.

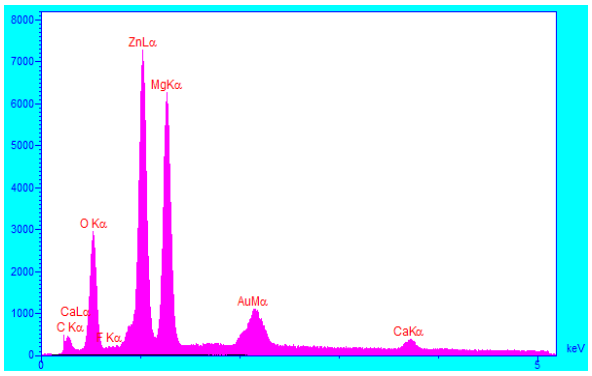

Fig. 4. EDS analysis of the synthesized Mg-4wt.% Zn scaffold.

3.2. Mechanical Properties of Scaffolds

Fig. 5. shows the microhardness changes of alloy scaffolds with increasing Zn content. It is known that with increasing Zn, the hardness of the samples has increased. Zn has increased hardness in two ways. First, by adding Zn to the Mg matrix, $MgZn_2$ and MgZn intermetallic precipitates are formed during sintering. These precipitates can prevent dislocation movement through the Orowan mechanism, which increases the hardness. However, further increase in the amount of Zn leads to its diffusion to the matrix and increases the hardness by creating a solid solution αMg matrix.

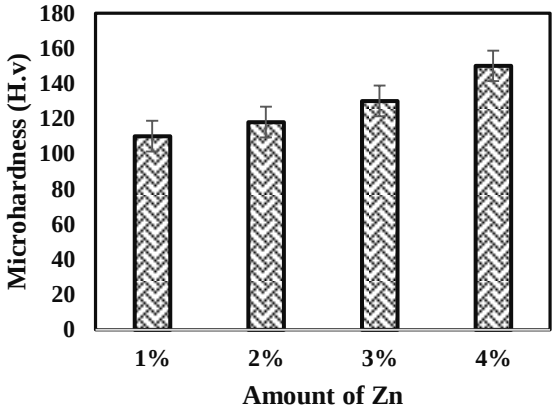

Fig. 5. Microhardness changes of scaffolds with increasing amount of Zn.

Fig. 6. illustrates the compressive strength of the sintered Mg-Zn scaffolds containing different Zn amounts. It can be seen that with the increase of Zn content and the formed nano Mg-Zn intermetallics, the compressive strength of the scaffolds increase. Zn element mainly resolves in primary magnesium when Zn content is 1%–2%, which can improve the compressive strength of the scaffold by solid-solution strengthening. When Zn content is 3%, many nano Mg-Zn intermetallics will precipitate from matrix, which enhances the strength by a dispersion strengthening mechanism [21].

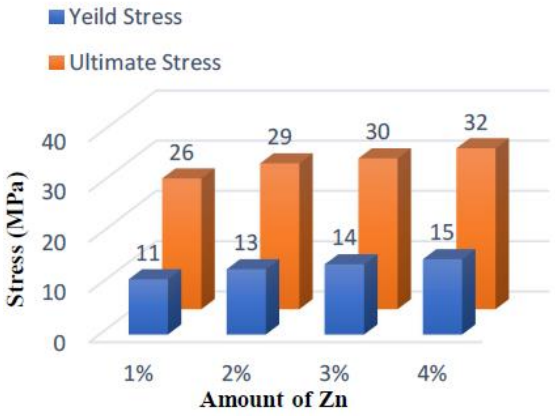

Fig. 6. The compressive strength of the synthesized scaffolds containing of different Zn amounts.

3.3. In Vitro Corrosion Properties of Scaffolds

Fig. 7. shows the electrochemical polarization curves of the sintered Mg-Zn scaffolds. The addition of Zn into Mg-Zn scaffolds can obviously move the corrosion potential and the pitting potential to be nobler, indicating that the Zn element can improve the stability of the passivation film and the corrosion resistance. The best corrosion resistance is obtained at 3% Zn.

When Zn content exceeds 3% the anti-corrosion property decreases. The change of the pitting potential in Table. 4. shows that adding Zn can move the pitting potential to a nobler value to some extent. It was reported that the addition of Zn in magnesium alloy could benefit the formation of a compact passive film [21]. The enrichment of Zn on the surface film can protect the magnesium scaffold from further corrosion. By comparing the Mg-4wt.% Zn scaffold with nanocomposite scaffold containing 3 wt. % Zn, the corrosion property is decreased. The probable reason might be that the volume fraction of Mg-Zn phases is higher in Mg-4wt.% Zn scaffold than that in Mg-3wt.% Zn scaffold. When Zn content is up to 3%, many nano $MgZn_2$ and MgZn phases precipitate from matrix, and act as cathode in the corrosion process, which accelerates the corrosion and reduces the anti-corrosion properties of magnesium.

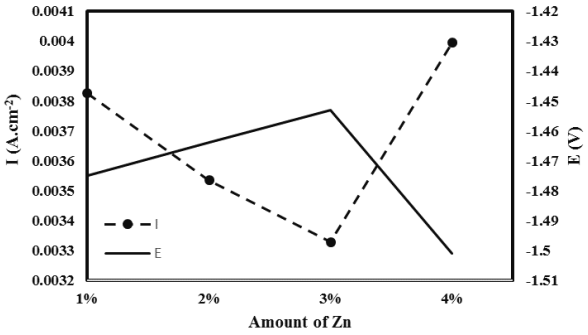

Fig. 7. Electrochemical parameters of the scaffolds obtained from the polarization curves.

4. Conclusion

1. Mg-Zn alloy scaffolds with macro pore size distribution in the range of 200-400 µm and nano $MgZn_2$ and MgZn intermetallics with size of 20 nm have been successfully fabricated via powder metallurgy process.
2. The mechanical property of the alloy scaffold can be improved by Zn element and formation of nano $MgZn_2$ and MgZn phases.
3. In vitro anti-corrosion property of the Mg-Zn alloy scaffolds can be effectively improved by Zn element when the content is less than 3 wt.%.

References

[1] C. H. Chang, F. H. Lin, T. F. Kuo and H. C. Liu, Cartilage tissue engineering. J. Biomed. Eng. Appl., Basis and Commun., 17, (2005), 1.
[2] M. V. Risbud and M. Sittinger, Tissue engineering: advances in in vitro cartilage generation. J. Trends in Biotech. 20, (2002), 351.
[3] J. Bonadio, E. Smiley, P. Patil and S. Goldstein, Localized, direct plasmid gene delivery in vivo: prolonged therapy results in reproducible tissue regeneration. J. Nat. Med., 5, (1999), 753.
[4] H. Y. Cheung, K. T. Lau, T. P. Lu, D. Hui, A. Critical Review on Polymer-Based Bio-Engineered Materials for Scaffold Development., J. Compos. Part B. (2007), 38:291.
[5] A. H. Yusop, A. A. Bakir, N. A. Shaharom, M. R. Abdul Kadir and H Hermawan, Porous biodegradable metals for hard tissue scaffolds: A review. Int. J. Biomater., 1, (2012), 1.
[6] N. E. L. Saris, E. Mervaala, H. Karppanen, J. A. Khawaja and A. Lewenstam, Magnesium: an update on physiological, clinical and analytical aspects., J. Clin. Chim. Acta., 294, (2000), 1.
[7]J. Vormann, Magnesium Nutrition Andmetabolis, J. Mol. Aspects Med., 24, (2003), 27.
[8] T. Okuma, Magnesium and bone strength. J. Nutr. 17: (2001), 679.
[9] M. P. Staiger, A. M. Pietak, J. Huadmai and G. Dias, J. Biomater., 27: (2006), 1728.
[10] F. Witte, V. Kaese, H. Haferkamp, E. Switzer, A. Meyer-Lindenberg, C. Wirth and H. Windhagen, J. Biomater., 26, (2005), 3557.
[11] Z. J. Li, X. N. Gu, S. Q. Lou, Y. F. Zheng, J. Biomater., 29, (2008), 1329.
[12] G. L. Song, J. Corros. Sci., 49: (2007), 1696.
[13] S. Gonzáleza, E. Pellicera, J. Fornella and A. Blanquer, J. Mech. Behave. Biomed. Mater. 6, (2012) 53.
[14] K. Abdelrazek Khalil, Process. Int. J. Electrochem. Sci. 7, (2012), 10698.
[15] C. J. Deng, M. L. Wong, M. W. Ho, P. Yu, H. L. Dickon, J. Composites Part A, 36, (2005), 551.
[16] X. Gu, Y. Zheng, S. Zhong and T. Xi, J. Biomater., 31, (2010), 1093.
[17] A. Kaya, D. Eliezer, G. Ben-Hamu, O. Golan, Y. G. Na and K. S. Shin, J. Met. Sci. Heat Treat. 48, (2006), 50.
[18] E. Zhang, D. Yin, L. Xu, L. Yang and K. Yang, J. Mater. Sci. and Eng. C, 29, (2009), 987.
[19] H. Zhuang, Y. Han and A. Feng, J. Mater. Sci. Eng. C 28, (2008), 1462.
[20] T. Kokubo and H. Takadama, J. Biomater., 27 (2006), 2907.
[21] Y. Dong-song, Z. Erlin and Z. Song-yan, J. Transe. Nonferrous Met. Soc. China, 18, (2008), 763.